

RESEARCH

Open Access



Single-cell transcriptome sequencing reveals the mechanism of Realgar improvement on erythropoiesis in mice with myelodysplastic syndrome

Hao Xu^{1,2†}, Kexin Hu^{1,2†}, Yanlu Wang^{1,2†}, Shuyang Cai^{1,2}, Fan Wu^{1,2}, Jizhang Bao^{1,2}, Qi Hu^{1,2}, Yu Guan^{1,2*}, Yuchen Tao^{1,2*} and Jiahui Lu^{1,2*}

Abstract

Myelodysplastic syndrome (MDS) is a malignant hematologic disorder with limited curative options, primarily reliant on hematopoietic stem cell transplantation. Anemia, a prevalent symptom of MDS, has few effective treatment strategies. Realgar, though known for its therapeutic effects on MDS, remains poorly understood in terms of its mechanism of action. In this study, both in vivo and in vitro experiments were conducted using Realgar and its primary active component, As_2S_2 , to examine their impact on mouse erythroblasts at the single-cell level. Realgar treatment significantly altered the transcriptional profiles and cellular composition of bone marrow in mice, both in vivo and in vitro. Differentially expressed genes in erythroblasts regulated by Realgar were identified, unveiling potential regulatory functions and signaling pathways, such as heme biosynthesis, hemoglobin production, oxygen binding, IL-17 signaling, and MAPK pathways. These findings suggest that Realgar enhances the differentiation of erythroblasts in mouse bone marrow and improves overall blood cell counts. This work offers preliminary insights into Realgar's mechanisms, expands the understanding of this mineral medicine, and may inform strategies to optimize its therapeutic potential in hematologic diseases.

Keywords Realgar, Myelodysplastic syndrome, MDS, Erythropoiesis

Introduction

Myelodysplastic syndrome (MDS) is a malignant hematopoietic neoplastic disorder characterized by a reduction in peripheral blood cells across one or more lineages, dysplastic hematopoiesis in the bone marrow, ineffective hematopoiesis, and a high risk of progression to acute myeloid leukemia (AML) [1, 2]. The 5-year progression rate from MDS to AML is estimated to range from 25 to 35%. Anemia is a predominant symptom in patients with MDS, with over 80% exhibiting hematopoietic dysfunction, primarily due to the presence of approximately 10% dysplastic erythrocytes in the bone marrow, leading to ineffective hematopoiesis. Severe impairment in terminal erythroid differentiation

[†]Hao Xu, Kexin Hu and Yanlu Wang contributed equally to this work.

*Correspondence:

Yu Guan
yuguan1976@163.com
Yuchen Tao
taoyc_tcm@126.com
Jiahui Lu
lujiahui_sci@126.com

¹ Clinical Hematology Center, Shanghai Municipal Hospital of Traditional Chinese Medicine, Shanghai University of Traditional Chinese Medicine, Shanghai, China

² Institute of Hematology, Shanghai Municipal Hospital of Traditional Chinese Medicine, Shanghai University of Traditional Chinese Medicine, Shanghai, China



has been identified as a robust, independent prognostic marker of poor overall survival in MDS [3]. As a condition marked by ineffective erythropoiesis, patients with MDS often experience transfusion dependence and significant iron overload [4]. Therefore, there is an urgent need for further research into alternative transfusion methods, as well as therapeutic agents or strategies that can promote erythroid differentiation in the bone marrow, ultimately improving patient prognosis.

The success of low-dose arsenic trioxide in the treatment of acute promyelocytic leukemia [5] has led to ongoing exploration of various arsenic compounds for treating hematologic malignancies, including MDS. In recent years, oral formulations containing Realgar (Xionghuang, in China) have demonstrated notable efficacy in MDS treatment, offering hope for many patients. Realgar has been incorporated into expert consensus and guidelines for the traditional Chinese medicine treatment of MDS [6, 7]. Research into the mechanisms underlying Realgar's therapeutic effects in MDS has been a focal point, with findings indicating that it can inhibit cell proliferation, induce apoptosis, modulate epigenetic modifications, and promote erythroid differentiation [8–10]. Recent studies by our group have revealed that Realgar induces apoptosis in MDS cells by inhibiting the STAT3/GLUT1 signaling pathway [11]. The primary active component of Realgar, As_2S_2 , has been shown to inhibit the growth of HL-60 cells, induce apoptosis, and promote erythroid differentiation in MDS and MDS/AML cell lines in vitro [12, 13]. Previous work by our team demonstrated that As_2S_2 can suppress the proliferation of bone marrow mononuclear cells in patients with MDS, induce apoptosis via histone acetylation modulation, reduce TLR2 activation, and enhance GATA-1 expression, thereby facilitating erythroid differentiation [14]. However, the precise mechanism by which Realgar promotes erythroid differentiation and improves ineffective hematopoiesis in MDS remains unclear.

Single-cell RNA sequencing (scRNA-seq) enables the analysis of transcriptomic features at the single-cell level, providing high-resolution insights into disease pathogenesis. This technology offers advanced detection capabilities, yielding more comprehensive and precise data for drug discovery, which may guide the identification of potential clinical applications [15]. In this study, scRNA-seq was employed to investigate the effects of Realgar and its active compound As_2S_2 on mouse bone marrow erythroid precursor cells, both in vivo and in vitro. Functional enrichment analysis of differentially expressed genes (DEGs) elucidated the mechanisms by which Realgar enhances erythroid differentiation and addresses ineffective hematopoiesis in MDS.

Materials and methods

Animal models and identification

SPF-grade NUP98-HOXD13 fusion gene mice (hereafter referred to as NHD13 mice) and five wild-type female C57BL/6 J mice, weighing 15–20 g, were used in this study. All mice were obtained from The Jackson Laboratory, USA, and had valid animal qualification certificates. Male and female mice were housed together in a 1:1 ratio for mating, with genotyping performed after the birth of the offspring. Protocols for identification and relevant details are provided in the Supplemental Materials and Methods (Supplementary Table S2). Genotyping results confirmed that NHD13-positive mice were categorized into the MDS model group, while the negative mice were assigned to the wild-type (WT) group. All animals were maintained in the SPF-grade barrier environment of the Experimental Animal Center at Shanghai Municipal Hospital of Traditional Chinese Medicine, operating under license number SYXK (Shanghai) 2020 - 0014. Mice were kept in a controlled environment with a 12-h light–dark cycle, a temperature of $(22 \pm 2)^\circ\text{C}$, and humidity of $(50 \pm 10\%)$, with free access to water. The animal experiments were approved by the Experimental Animal Ethics Committee of the Municipal Hospital of Traditional Chinese

(See figure on next page.)

Fig. 1 Therapeutic efficacy of Realgar in the murine MDS model (NUP98-HOXD13). **(A)** Complete blood count (CBC) analysis of peripheral blood from wild-type, NHD13, and Realgar-treated mice ($n = 5$). WBC, white blood cells; RBC, red blood cells; HB, hemoglobin; PLT, platelets. **(B)** Histopathological examination of liver, spleen, heart, and kidney tissues from each group. Sections were stained with H&E. Scale bar, 200 μm . **(C)** Body weight changes in WT, murine MDS model, and Realgar-treated mice during the treatment period. Data are presented as mean \pm SD ($n = 5$). **(D)** Quantification of colony formation in cultures of nucleated BM or spleen cells isolated from WT, NHD13, or Realgar-treated groups, cultured in BFU-E medium for 12 days or CFU-E medium for 2 days. Data are presented as mean \pm SEM ($n = 3$). **(E)** (Left) Flow cytometric analysis of erythroblasts in BM of the three groups. Erythroblasts were classified into four subpopulations based on surface staining for CD71 and Ter-119: Ter-119^{med}CD71^{high} proerythroblasts (R1), Ter-119^{high}CD71^{high} basophilic erythroblasts (R2), Ter-119^{high}CD71^{med} late basophilic and polychromatophilic erythroblasts (R3), and Ter-119^{high}CD71^{low} orthochromatophilic erythroblasts (R4). **(F)** (Right) Quantification of the percentages of R1–R4 populations shown in the left panel. Data are presented as mean \pm SEM ($n = 5$). (*, $P < 0.05$; **, $P < 0.01$; ***, $P < 0.001$; n.s., not significant)

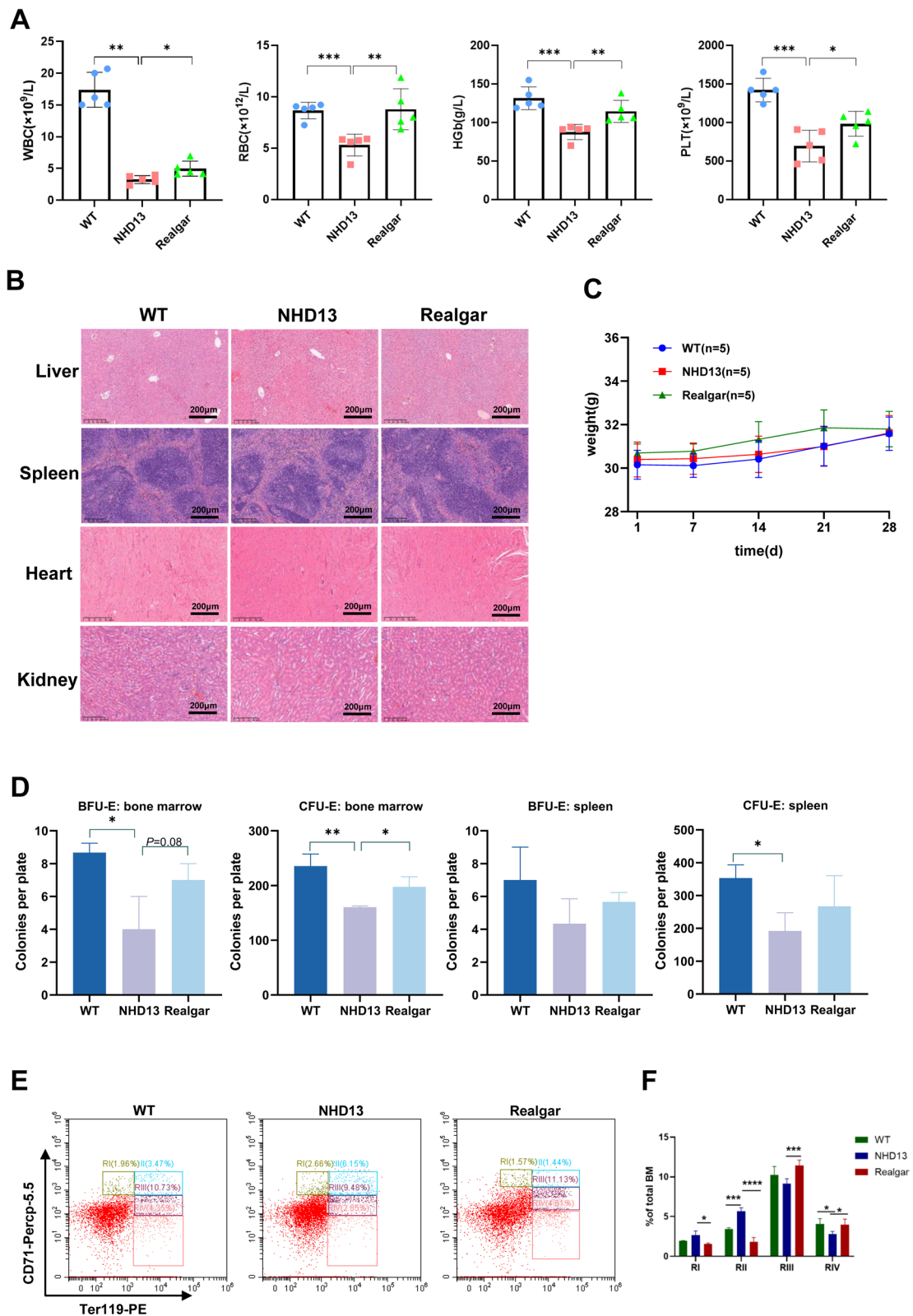


Fig. 1 (See legend on previous page.)

Medicine affiliated with Shanghai University of Traditional Chinese Medicine.

Group assignment and drug administration

The NHD13 mice were randomly divided into two groups: the model control group (NHD13) and the Realgar intervention group, with 5 mice per group. Dosing was calculated based on the body weight conversion coefficient table [16]. Realgar was prepared as a suspension in 0.5% sodium carboxymethyl cellulose, and the Realgar intervention group received an oral dose of 120 mg kg⁻¹ d⁻¹. The model control group was administered 200 µl of 0.5% sodium carboxymethyl cellulose daily. All mice were treated continuously for one month. As₂S₂, purchased from Sigma-Aldrich, was dissolved in 1 N NaOH, and the pH was adjusted to 7.35–7.45 with HCl to obtain a final concentration of 0.5 mM. The solution was filtered through a 0.20 µm membrane filter (Advantec Co., Japan) and stored at –20 °C until use. Further details on As₂S₂ and other materials are presented in the Supplementary Table S1.

Bone marrow cell purification and isolation of Ter119⁺ cell

Mice were euthanized via cervical dislocation, and their bilateral legs were amputated. The skin and muscles were removed to expose the bones, which were then placed in a 6-well plate containing 2% fetal bovine serum (FBS, Gibco, catalog number: 10099 - 141). Bone marrow was flushed out from the cavity using a 1 ml syringe on ice until the bones became translucent. The bone marrow suspension was filtered through a 70 µm filter and transferred to a 15 ml centrifuge tube, which was then centrifuged at 300 g for 10 min, discarding the supernatant. The cells were lysed twice with red blood cell lysis buffer and washed once with PBS (Beyotime, catalog number: C0221 A). The resulting single-cell suspension was filtered through a 40 µm filter (Bkman, catalog number: 110426003). Cell viability and concentration were assessed using a cell counter (Countstar, Shanghai, China). The cells passed quality control and were prepared for single-cell analysis. Ter119⁺ cells were enriched using magnetic beads following the manufacturer's protocol (Miltenyi Biotec, Bergisch-Gladbach, Germany).

Cell culture and treatment

Bone marrow cells from mice were cultured in Iscove's Modified Dulbecco Medium (IMDM) supplemented with 10% fetal bovine serum (Thermo, Waltham, MA, USA), 100 U/ml penicillin, 100 µg/ml streptomycin (Thermo), and 20 ng/ml IL-3, SCF, and Flt3 at 37 °C in a 95% air/5% CO₂ atmosphere. K562 cells, purchased from FuHeng Biology (Shanghai, China), were cultured according to the manufacturer's instructions. For erythroid induction, K562 cells were treated with 30 µM Hemin for 48 h, and As₂S₂ was applied at a concentration of 625 nM.

Histopathological analysis

Body weight and clinical signs were recorded every two days. Following euthanasia, liver, spleen, heart, lung, and kidney tissues were immediately fixed in 10% formalin at room temperature for 24 h. The tissues were then embedded in paraffin, sectioned, and mounted on glass microscope slides. Hematoxylin and eosin staining was performed, and the sections were examined using light microscopy by two independent researchers blinded to the randomization scheme.

Flow cytometry analysis

For single-cell flow cytometry, bone marrow cells were prepared as previously described in Bone marrow cell purification. After red blood cell lysis and removal, cells were washed and resuspended in a staining buffer. Fc block was applied for 10 min on ice to reduce non-specific immunofluorescent staining. For cell surface marker detection (Ter119, CD71), cells were resuspended in 100 µl staining buffer, stained with primary antibodies for surface markers for 30 min at 4 °C in the dark, and washed twice with staining buffer. Cell pellets were resuspended in the staining buffer for flow cytometry analysis (Cytoflex Lx, Beckman Coulter), with gates and compensations set prior to each experiment. All antibodies used are listed in the Supplemental Information (Table S1). The experiment was repeated more than three times.

(See figure on next page.)

Fig. 2 Single-cell atlas of bone marrow cells across three groups (In vivo). **(A)** Flowchart illustrating the research process for single-cell RNA sequencing. **(B)** Thirty-four bone marrow cell clusters. UMAP representation of unbiased clustering of all bone marrow cells from the three groups (combined bone and bone marrow fractions, n = 5 mice). **(C)** UMAP representation of unbiased clustering and cell annotation for bone marrow cells from the three groups. A total of 12 cell types were identified. **(D)** Cluster signature genes are highlighted on the left. Average expression of the top differentially expressed genes (rows) across the cells (columns), with warmer colors indicating higher expression. **(E)** UMAP plot displaying the distribution of representative markers for each cell type. Color represents the relative expression level of each gene. **(F)** Proportions of each cell type

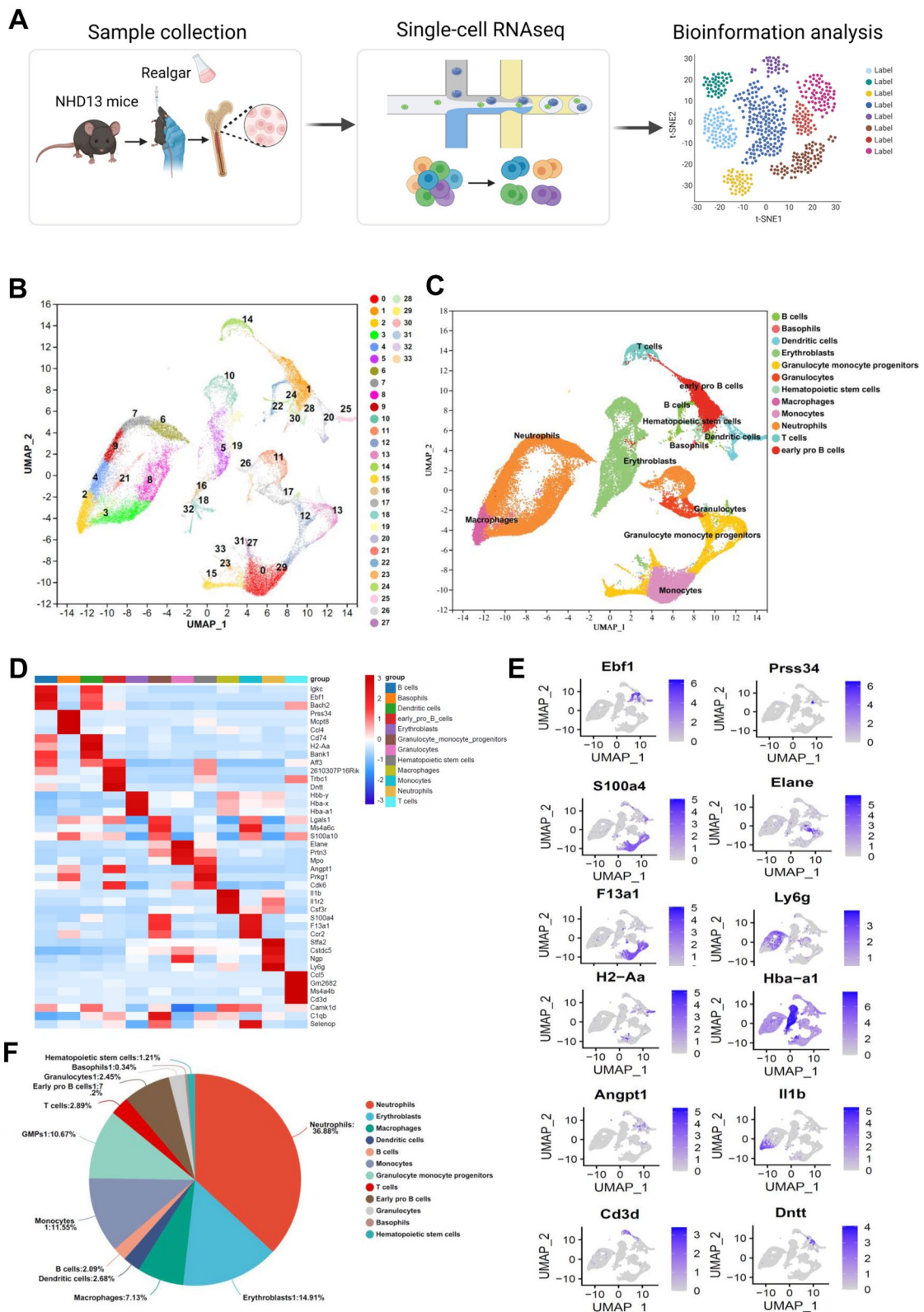


Fig. 2 (See legend on previous page.)

Erythroid burst-forming units and colony-forming units

Mice were euthanized by cervical dislocation, and peripheral blood, spleen, tibias, and femurs were collected. Peripheral blood was used for complete blood counts, while spleen and bone marrow cells were isolated and plated in methylcellulose-based media to assess clonogenic progenitors of the erythroid lineage. Colony-forming unit-erythroid (CFU-E) assays were performed by culturing bone marrow and spleen cells at 1×10^5 and 2×10^5 cells/ml, respectively, in methylcellulose medium containing recombinant erythropoietin (rmEPO; Methocult M3334, Stem Cell Technologies), with colonies counted independently by two investigators on day 2. For burst-forming unit-erythroid (BFU-E) assays, bone marrow and spleen cells were cultured at 2.5×10^4 and 2.5×10^5 cells/ml, respectively, in methylcellulose medium containing recombinant stem cell factor (rmSCF), recombinant interleukin-3 (rmIL-3), recombinant interleukin-6 (rmIL-6), and recombinant erythropoietin (rmEPO; Methocult M3434, Stem Cell Technologies), with colonies counted similarly on day 12.

Western blot

Western blot (WB) was performed following standard protocols. In brief, cell lysis was carried out using RIPA buffer (Beyotime) containing protease and phosphatase inhibitors. After protein quantification, the lysates were resuspended in a 5X protein loading buffer and loaded onto SDS-PAGE gels. Proteins were transferred to Immobilon polyvinylidene fluoride (PVDF) membranes. Primary antibodies used in the study were as follows: S100 A8 (Abcam, ab92331; 1:1000), S100 A9 (Abcam, ab242945; 1:1000), ERK1/2 (Cell Signaling Technology, 9102S, 1:1000), phosphorylated ERK1/2 (Cell Signaling Technology, 4370S, 1:1000), GAPDH (Cell Signaling Technology, 5174, 1:1000), and β -actin (Abcam, ab156302; 1:1000). Membranes were incubated with HRP-conjugated secondary antibodies and developed using ECL chemiluminescence substrates.

Single-cell RNA sequencing

Beads with unique molecular identifier (UMI) and cell barcodes were loaded close to saturation, so that each

cell was paired with a bead in a Gel Beads-in-emulsion (GEM). After exposure to cell lysis buffer, polyadenylated RNA molecules hybridized to the beads. Beads were retrieved into a single tube for reverse transcription. On cDNA synthesis, each cDNA molecule was tagged on the 5' end (that is, the 3' end of a messenger RNA transcript) with UMI and cell label indicating its cell of origin. Briefly, $10 \times$ beads that were then subject to second-strand cDNA synthesis, adaptor ligation, and universal amplification. Sequencing libraries were prepared using randomly interrupted whole-transcriptome amplification products to enrich the 3' end of the transcripts linked with the cell barcode and UMI. All the remaining procedures including the library construction were performed according to the standard manufacturer's protocol (Chromium Single Cell 3' v3.1). Sequencing libraries were quantified using a High Sensitivity DNA Chip (Agilent) on a Bioanalyzer 2100 and the Qubit High Sensitivity DNA Assay (ThermoFisher Scientific). The libraries were sequenced on NovaSeq6000 (Illumina), and 150 bp paired-end reads were generated. The sequencing and bioinformatics analysis were performed by Majorbio Co., Ltd (Shanghai, China).

Single cell RNA-seq data processing

Reads were processed using the Cell Ranger 4.0 pipeline with default and recommended parameters. FASTQs generated from Illumina sequencing output were aligned to the mouse genome, version GRCm38, using the STAR algorithm [17]. Next, Gene-Barcode matrices were generated for each individual sample by counting UMIs and filtering non-cell associated barcodes. Finally, we generate a gene-barcode matrix containing the barcoded cells and gene expression counts. This output was then imported into the Seurat (v3.2.0) R toolkit for quality control and downstream analysis of our single cell RNAseq data [18]. All functions were run with default parameters, unless specified otherwise. We first filtered the matrices to exclude low-quality cells using a standard panel of three quality criteria: (1) number of detected transcripts (number of unique molecular

(See figure on next page.)

Fig. 3 Bone marrow erythroblasts cell types defined by scRNA-seq. **(A)** UMAP plot displaying eleven subclusters of bone marrow erythroblasts. **(B)** Heatmap illustrating discriminative gene sets for each cluster, with a cutoff threshold of $FDR < 0.01$ and $|\log FC| > 0.25$. **(C)** Cell differentiation trajectory reconstructed using Monocle. Each dot represents a single cell, with colors indicating different cell clusters. **(D)** UMAP plot colored by expression levels of *Mki67* (Left) and *Bpgm* (Right). **(E)** Cell cycle phases identified using Seurat. Phases are depicted in different colors: G1 in green, S in blue, and G2/M in red. **(F)** UMAP plot showing the distribution of erythroblast differentiation stages. ProE, BasoE, PolyE, and OthoE are represented in distinct colors. **(G)** Enriched GO terms and *P*-values for the four stages of cells. **(H)** Proportions of the four cell types in WT, NHD13, and Realgar groups

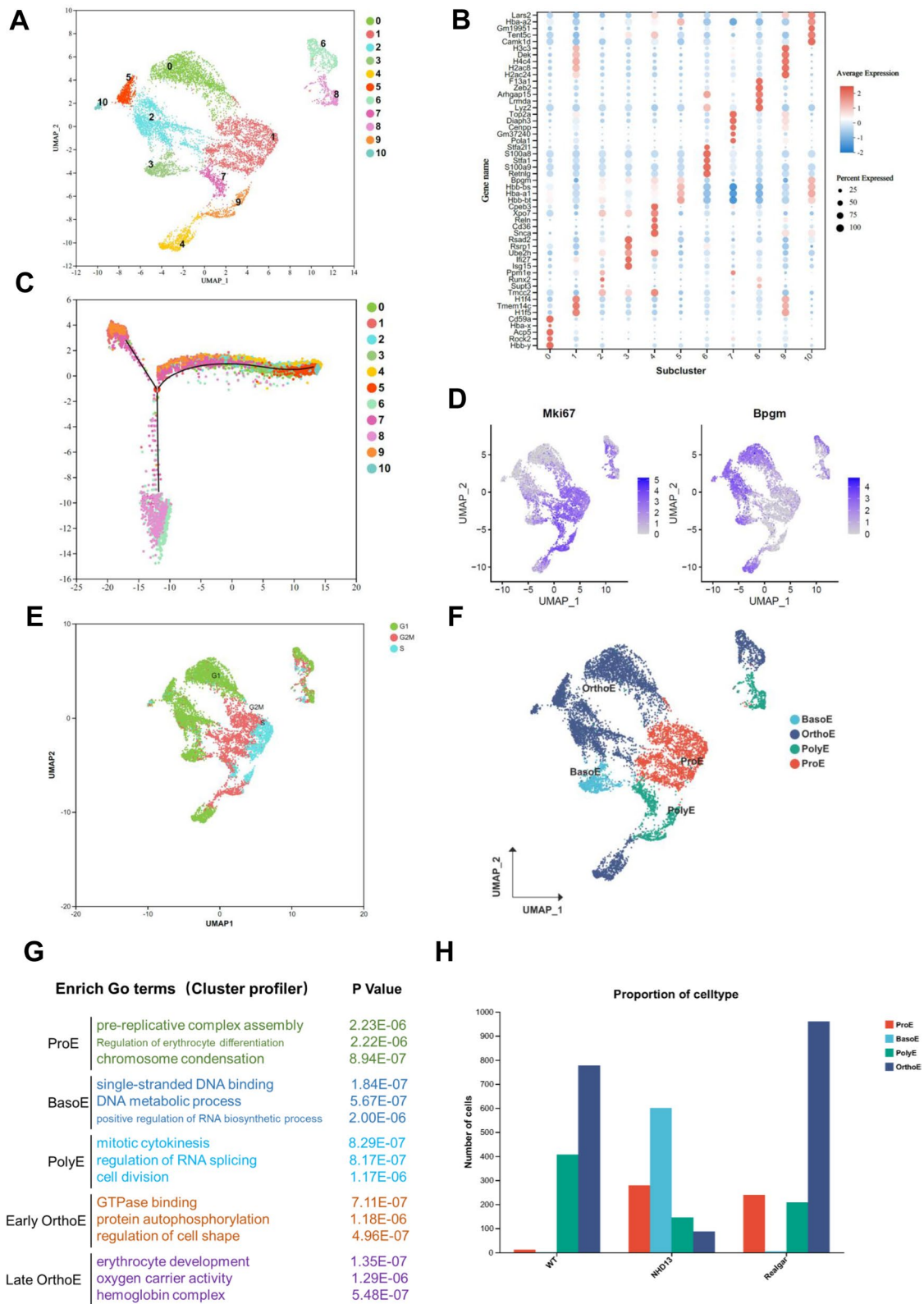


Fig. 3 (See legend on previous page.)

identifiers); (2) detected genes; and (3) percent of reads mapping to mitochondrial genes (Quartile threshold screening criteria). The expression of mitochondria genes was calculated using Percentage FeatureSet function of the *seurat* package. The normalized data (Normalize Data function in *Seurat* package) was performed for extracting a subset of variable genes. Variable genes were identified while controlling for the strong relationship between variability and average expression. Next, we integrated data from different samples after identifying ‘anchors’ between datasets using Find Integration Anchors and Integrate Data in the *seurat* package [19]. Then we performed principal component analysis (PCA) and reduced the data to the top 30 PCA components after scaled the data. We visualized the clusters on a 2D map produced with t-distributed stochastic neighbor embedding (t-SNE) [20].

Identification of cell types and subtypes by nonlinear dimensional reduction (t-SNE)

Cells were clustered using graph-based clustering of the PCA reduced data with the Louvain Method [21] after computing a shared nearest neighbor graph. For sub-clustering, we applied the same procedure of scaled, dimensionality reduction, and clustering to the specific set of data (usually restricted to one type of cell.) For each cluster, we used the Wilcoxon Rank-Sum Test to find significant differentially expressed genes comparing these remaining clusters. SCINA and known marker genes were used to identify cell type [22].

Differential expression analysis and functional enrichment

To identify DEGs (differential expression genes) between two different samples or clusters, was performed using the function FindMarkers in *Seurat*, using a likelihood ratio test. Essentially, DEGs with $|\log_2 \text{FC}| > 0.25$ and Q value ≤ 0.05 were considered to be significantly different expressed genes. In addition, functional-enrichment analysis GO were performed to identify which DEGs were significantly enriched in GO terms and metabolic pathways at Bonferroni-corrected P -value ≤ 0.05 compared with the whole-transcriptome background. GO functional enrichment analysis was carried out by Goatools (<https://github.com/tanghaibao/Goatools>).

Statistical analysis

SPSS15.0 Statistics software was used for statistical data analysis. Student’s t-test or one-way analysis of variance (ANOVA) was used to compare statistics between two or more groups, $P < 0.05$ was considered statistically significant.

Results

Therapeutic efficacies of realgar in a murine MDS model

NHD13 mice were employed as a model for MDS in this study. Widely recognized for their robust penetrance and reproducibility, these mice closely mirror human MDS pathology, exhibiting peripheral blood cell reduction, aberrant bone marrow proliferation, and clinical disease progression. Within 7–14 months, NHD13 mice may progress to acute leukemia or die due to anemia or decreased blood cell count caused by advanced-stage MDS [23]. The model mice underwent fusion gene identification (Supplementary Fig. S1). Compared to wild-type controls, the NHD13 mice exhibited a marked reduction in peripheral blood cell counts across all three lineages (Fig. 1A, * $P < 0.05$, ** $P < 0.01$, *** $P < 0.001$), confirming the model’s fidelity in replicating the human MDS pathological condition and meeting established diagnostic criteria for MDS model mice [24, 25]. Following one month of Realgar treatment, mice in the treatment group showed significant increases in WBC, RBC, Hb, and PLT counts, approaching normal levels (Fig. 1A, Supplementary Table S3), consistent with prior studies [26]. Histopathological analysis of the heart, liver, spleen, and kidneys revealed no significant organ changes between the groups (Fig. 1B). Moreover, Realgar treatment did not affect body weight in NHD13 mice (Fig. 1C, Supplementary Table S4). These results demonstrate that Realgar treatment in the NHD13 model is both effective and safe, without inducing adverse effects.

Given the observed enhancement of the erythroid lineage by Realgar, assays for BFU-E and CFU-E were performed to assess early progenitor cell numbers in the bone marrow and spleen of NHD13 mice (Fig. 1D). A significant decrease in both BFU-E and CFU-E was observed in the bone marrow of NHD13 model mice compared to the wild-type group ($P < 0.05$, $P < 0.01$). In contrast, CFU-E numbers in the Realgar-treated group increased

(See figure on next page.)

Fig. 4 Arsenic disulfide promotes erythroid differentiation of mouse bone marrow cells in vitro. **(A)** Flowchart outlining the research process to investigate the effect of arsenic disulfide. **(B)** Mouse bone marrow cells were cultured for 48 h or 10 days (as indicated) with 625 nM As_2S_2 . Expression of CD71 and Ter119 was assessed by flow cytometry. **(C)** Quantification of the percentages of $\text{CD71}^+\text{Ter119}^+$ populations shown in the left panel. Data are presented as mean \pm SEM ($n = 3$). **(D)** K562 cells were cultured for 48 h (as indicated) with 30 μM hemin or 625 nM As_2S_2 . Expression of CD71 and CD235a was analyzed by flow cytometry. **(E)** Quantification of the percentages of $\text{CD71}^+\text{CD235a}^+$ populations shown in the left panel. Data are presented as mean \pm SEM ($n = 3$)

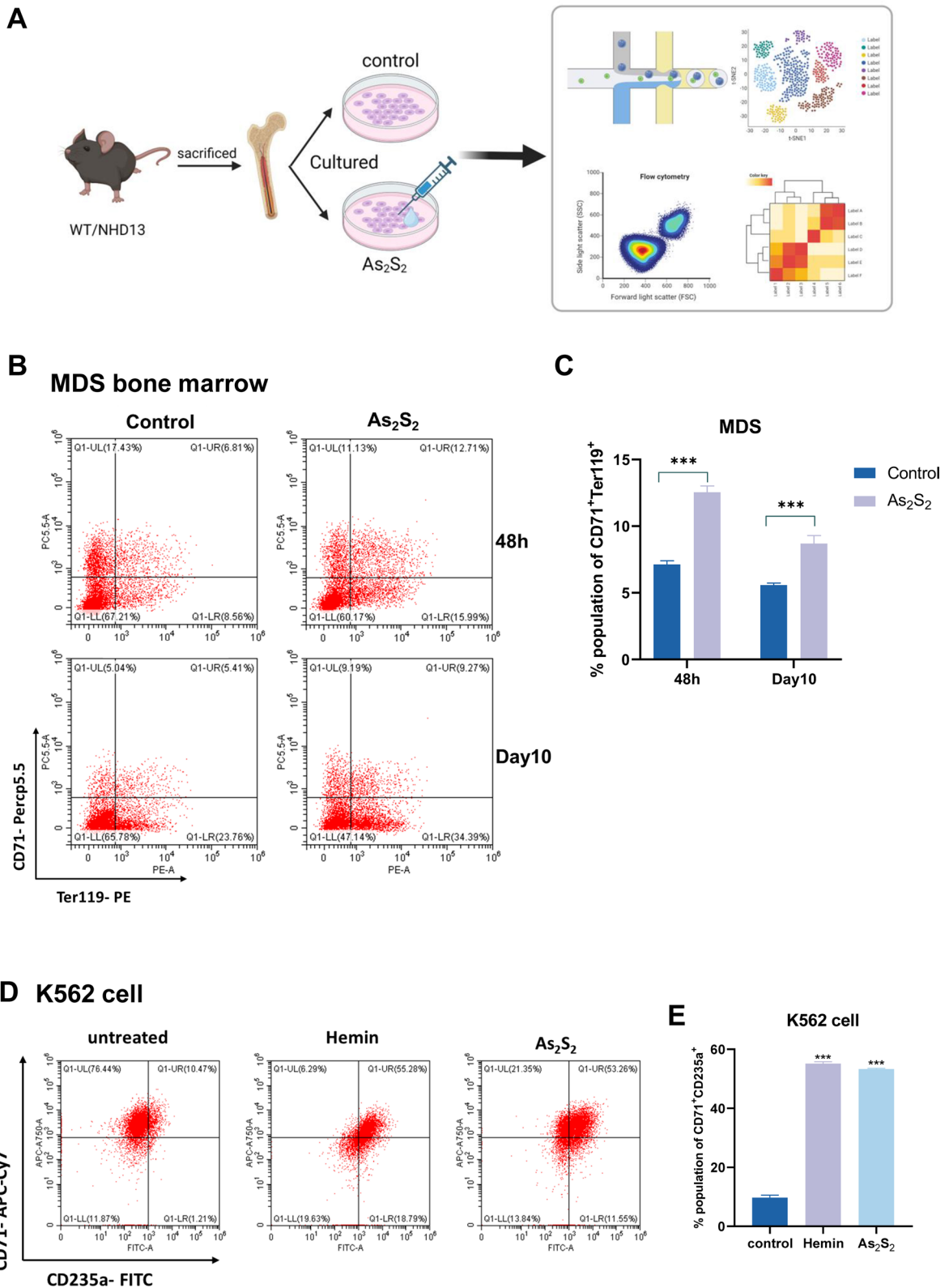


Fig. 4 (See legend on previous page.)

relative to the NHD13 group ($P < 0.05$), although no significant difference in BFU-E was observed, showing a rising trend ($P = 0.08$). In the spleen, CFU-E numbers in NHD13 mice were reduced compared to wild-type mice ($P < 0.05$), and while BFU-E numbers did not differ significantly from the wild-type group, a decreasing trend was observed. Realgar treatment resulted in a slight increase in both BFU-E and CFU-E in the spleen relative to the NHD13 group, though this difference lacked statistical significance, suggesting that Realgar primarily targets bone marrow progenitors and has a minimal impact on extramedullary hematopoiesis. Flow cytometric analysis using CD71 and Ter119 antibodies further revealed that Realgar treatment promotes the maturation of terminal erythroid progenitors in the bone marrow of NHD13 model mice (Fig. 1E, F).

Single-cell transcriptome atlas of bone marrow cells in NHD13 mice treated with realgar intervention

To elucidate the mechanism underlying the effects of Realgar treatment in MDS model mice, single-nucleus RNA sequencing was performed on bone marrow samples from 5 mice in each group, following the aforementioned experimental methods. Single-cell transcriptome analysis was conducted on 9,869 cells from WT mice, 11,766 cells from NHD13 mice, and 15,891 cells from the Realgar treatment group (Fig. 2A, Supplementary Table S5). Cell quality control was performed using Cell Ranger, and subsequent filtering using the quartile method excluded low-quality genes, mitochondria, and doublets, while cells expressing fewer than 200 genes were also excluded (Supplementary Table S6, Supplementary Fig. S2 A). Unsupervised clustering identified 34 distinct cell clusters across the samples (Fig. 2B). Based on a reference dataset and specific marker genes, cell types were categorized, including B cells, basophils, dendritic cells, erythroblasts, monocytes, granulocytes, hematopoietic stem cells, macrophages, granulocyte-monocyte progenitors, neutrophils, T cells, and early pro-B cells (Fig. 2C). Each cell type was reliably distinguished by its marker gene expression: (1) Erythroblasts (clusters 5, 10, 16, 19, 31) expressed *Hbb-y*, *Hba-x*, *Hba-a1*; (2) Neutrophils (clusters 3, 4, 6, 7, 8, 9, 11, 26) expressed *Ly6 g*, *Ngp*, *Cstdc5*; (3) Hematopoietic

stem cells (cluster 24) expressed *Angpt1*, *Prkg1*, *Cdk6*; (4) Granulocytes (cluster 17) expressed *Elane*, *Prtn3*, *Mpo*; (5) Monocytes (clusters 0, 29) expressed *S100a4*, *F13a1*, *Ccr2*; (6) Macrophages (cluster 2) expressed *Il1b*, *Il1r2*, *Csf3r*; and (7) Granulocyte-monocyte progenitors (clusters 12, 13, 27) expressed *Lgals1*, *Ms4a6c*, *S100a10* (Fig. 2D, Supplementary Table S7). To further refine cell type identification, marker gene distributions were visualized in a UMAP plot (Fig. 2E). The distribution and proportions of cell types across samples were also plotted (Fig. 2F, Supplementary Fig. S3), with neutrophils being the most abundant (36.88%), followed by erythroblasts. In addition, compared with the model group, the proportion of CD34⁺ cells increased in the Realgar group (5.53% vs. 13.76%), as did the proportion of CD45⁺ cells (82.74% vs. 90.27%), while the proportion of CD38⁺ cells decreased (1.05% vs. 0.52%, Supplementary Table S8, Supplementary Fig. S4). Given the observed improvements in blood counts, future analyses will primarily focus on erythroblasts.

Bone marrow erythroblasts subcluster defined by scRNA-seq

We performed unsupervised clustering on the Erythroblasts cell population and divided it into 11 clusters (Fig. 3A, Supplementary Dataset S1). The top 5 characteristic genes of each cluster were visualized using a bubble plot (Fig. 3B), with filtering conditions set at $FDR < 0.01$ and $|\log FC| > 0.25$. To determine the order of cell differentiation processes, we reconstructed the cell differentiation trajectory using Monocle. The results showed the differentiation order of cells within the clusters as follows: (8,1) → 7 → 9 → (0,2,3,5,6) → (4,10) (Fig. 3C). In other words, the cluster (8,1) represents the earliest stage of cell differentiation, while the cluster (4,10) represents a very late stage of differentiation. Additionally, the mRNA expression of *Bpgm*, a unique marker for red blood cells, is upregulated along the cell maturation pathway [27]. When comparing the *Bpgm* mRNA expression levels among these clusters, the values were higher in clusters (0,2,3,5,6) and (4,10) (Fig. 3D), indicating that clusters (0,2,3,5,6) and (4,10) may represent the later stages of differentiation. Furthermore, based on the expression of marker genes

(See figure on next page.)

Fig. 5 Single-cell atlas of bone marrow cells in control and As_2S_2 groups (in vitro). **(A)** t-SNE plot showing unbiased clustering of all bone marrow cells in the control and As_2S_2 groups, revealing 18 distinct cell clusters. **(B)** t-SNE plot of unbiased clustering and cell annotation of bone marrow cells in control and As_2S_2 groups. A total of 10 cell types were identified. **(C)** Bubble chart displaying the top 3 markers for each cell type. Dot size corresponds to the percentage of cells in which the gene is detected, and color indicates the average expression level of the gene in each cell type. **(D)** t-SNE plot showing the distribution of representative markers for each cell type. Color represents the relative expression level of each gene. **(E)** Proportions of each cell type

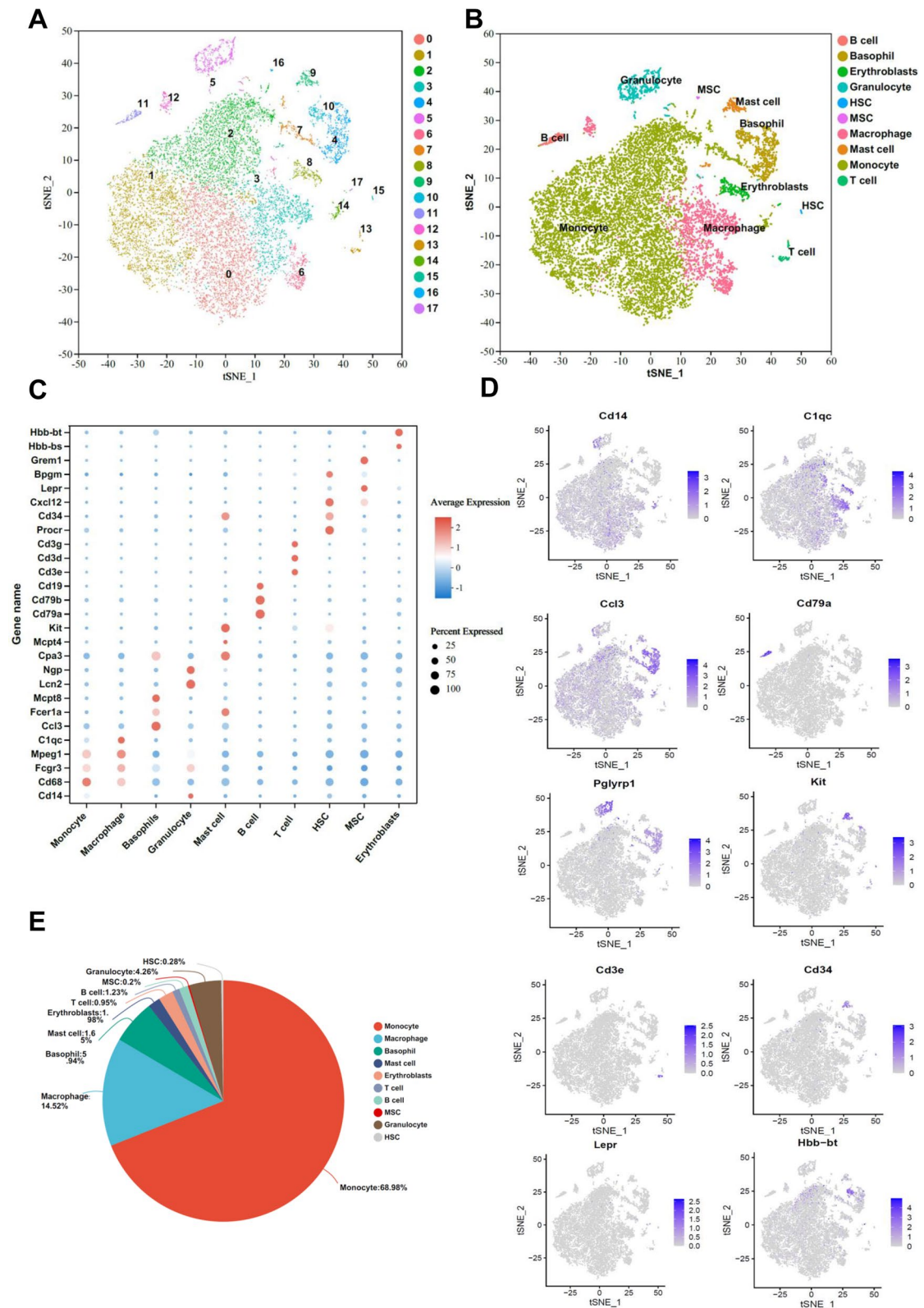


Fig. 5 (See legend on previous page.)

during the terminal differentiation process of mouse erythroid lineage, as reported previously (Supplementary Table S9), we identified cells in the differentiation stage corresponding to ProE, BasoE, PolyE, and OrthoE [28] using the Seurat software. We found that 59.75% of cells belonged to OrthoE, 20.98% of cells belonged to ProE, and a few PolyE and BasoE cells were also identified (Fig. 3F). This distribution of cells in different differentiation stages is consistent with previous reports [29] and with the developmental program of the mouse erythroid lineage in the bone marrow. OrthoE cells can be divided into an early stage (clusters 0, 2, 3, 5, 6) and a late stage (clusters 4, 10) of development. We also observed that compared to other stages, Mki67 mRNA expression is higher in the early stages of ProE and BasoE (Fig. 3D). Using the Seurat software, we found that 11.4% of cells were in the S phase, 28.9% of cells were in the G2/M phase, and 59.6% of cells were in the G1 phase. Further analysis revealed that ProE cells were mostly in the S phase, BasoE and PolyE cells were mostly in the G2/M phase, and early-/late- OrthoE cells were mostly in the G1 phase (Fig. 3E).

We performed Gene Ontology (GO) analysis based on differentially expressed genes among the five groups (ProE, BasoE, PolyE, early-OrthoE, and late-OrthoE) and identified associated enriched GO terms to gain insights into the biological processes (Supplementary DatasetS2). A set of 1905 signature genes was identified in cluster 1 and 8 representing ProE, the GO terms for this cluster were significantly enriched for differentially expressed genes related to pre-replicative complex assembly, Regulation of erythrocyte differentiation and chromosome condensation. BasoE cells with 374 differential expressed genes ($|\log_{2}FC| > 0.5$, $FDR < 0.01$), which were for single-stranded DNA binding, DNA metabolic process, positive regulation of RNA biosynthetic process. For early-OrthoE stage, 1088 differentially expressed genes were identified, including GTPase biological synthesis and regulation of cell shape. At late-OrthoE stage, a transition period before generation of enucleate reticulocytes, differentially expressed genes related to erythrocyte development and hemoglobin complex synthesis were significantly enriched (Fig. 3G).

These results provide a more comprehensive map of mouse bone marrow erythroid progenitor cells, allowing us to have a more comprehensive understanding of NHD13 mouse bone marrow. In addition, we analyzed the proportion of erythroid progenitor cells in each group (Fig. 3H). The proportion of ProE was highest in the NHD13 group and lowest in the WT group, with a decrease in the Realgar group compared to the model group. The proportion of OrthoE decreased in the NHD13 group and increased in the Realgar group, consistent with the flow cytometry results previously obtained (Fig. 1E, F). These results suggest that realgar can promote the maturation and differentiation of late-stage erythroid progenitor cells in mice.

As₂S₂ promotes the in vitro erythroid differentiation of mouse bone marrow cells

To investigate the mechanism underlying Realgar treatment in MDS mice, in vitro experiments were performed using As₂S₂, the primary component of Realgar. Bone marrow cells from WT and NHD13 mice were isolated and cultured with As₂S₂. The effects of As₂S₂ on erythroid differentiation in cultured mouse bone marrow cells were assessed using flow cytometry and single-cell transcriptome sequencing (Fig. 4A). Flow cytometric analysis revealed that As₂S₂ treatment significantly increased the proportion of erythroid double-positive cells (CD71⁺Ter119⁺) in MDS mouse bone marrow cultures after 48 h and on day 10 (Fig. 4B, C), indicating that As₂S₂ promotes erythroid differentiation in vitro in MDS model mice. This effect was not observed in WT mice (Supplementary Fig. S5), suggesting that the erythroid differentiation-enhancing effect of As₂S₂ is specific to MDS pathologic clones and does not occur in normal clones. This phenomenon aligns with the traditional Chinese medicine principle of “using poison to counteract poison,” where toxic agents are utilized to target and eliminate cancerous toxins. To further validate this observation, the K562 chronic myeloid leukemia cell line, known for its capacity to spontaneously differentiate into erythroid cells and megakaryocytes [30], was used. As₂S₂ treatment significantly increased the proportion of erythroid markers CD235a⁺ and CD71⁺ ($P < 0.001$), indicating

(See figure on next page.)

Fig. 6 Enrichment analysis of differentially expressed genes in erythroblasts from in vivo experiments. **(A)** Volcano plot showing DEGs, with red dots indicating significantly upregulated genes ($P \leq 0.05$, $|\log_{2}FC| \geq 0.25$) and blue dots representing significantly downregulated genes ($P \leq 0.05$, $|\log_{2}FC| \geq 0.25$). The top 10 DEGs are labeled. **(B)** Venn diagram illustrating the overlap of upregulated DEGs in erythroblasts between the WT vs. NHD13 and Realgar vs. NHD13 comparisons, revealing 17 overlapping genes. **(C)** GO enrichment analysis of upregulated DEGs in the Realgar vs. NHD13 comparison. **(D)** Enrichment plot from Gene Set Enrichment Analysis (GSEA) comparing differentially regulated genes in the Realgar group versus the NHD13 group. GSEA was conducted using GSEA software (v4.1.0) and MSigDB, with one-sided statistical tests and adjustments for multiple comparisons. Black bars represent individual genes, and enrichment is indicated in green. Normalized enrichment score (NES) is displayed. **(E)** KEGG enrichment analysis of upregulated DEGs in the Realgar vs. NHD13 comparison

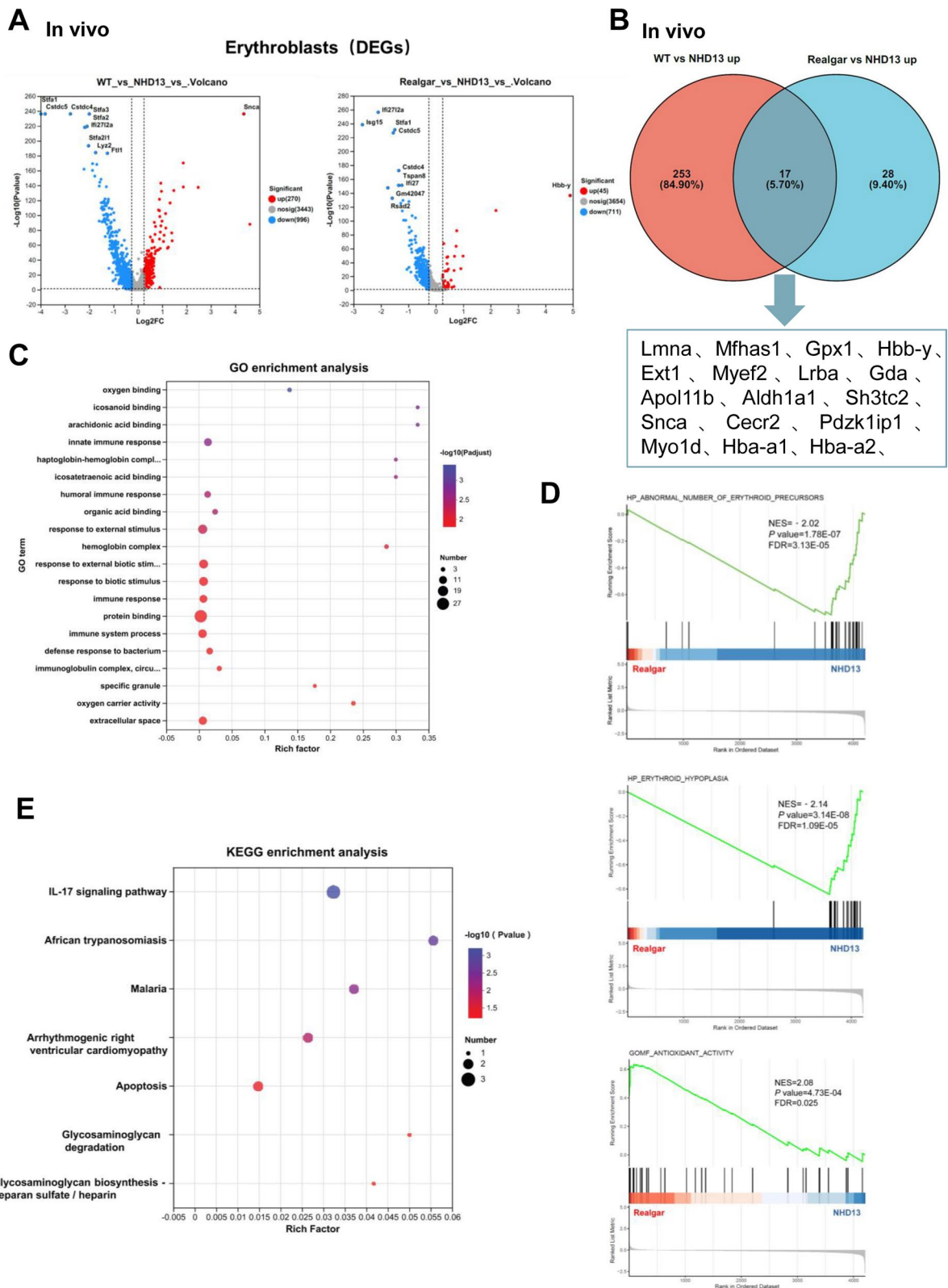


Fig. 6 (See legend on previous page.)

that As_2S_2 promotes erythroid differentiation in K562 cells, similar to the positive control Hemin (Fig. 4D, E).

Single-cell transcriptome atlas of bone marrow cells cultured in vitro with As_2S_2 intervention

To elucidate the in vitro mechanism by which As_2S_2 promotes erythroid differentiation in mouse bone marrow cells, single-cell transcriptome analysis was performed on As_2S_2 -treated and control mouse bone marrow cells using the aforementioned experimental methods. Cell quality control was performed with Cell Ranger, followed by filtering of genes, mitochondria, and doublets using the quartile method (Supplementary Fig. S2B). Cells with fewer than 200 genes were excluded, resulting in a final dataset comprising 7687 cells from the Control group and 6,735 cells from the As_2S_2 group (Supplementary Tables S10 and S11). After unbiased clustering, 18 distinct cell clusters were identified (Fig. 5A). Cell types were assigned based on reference datasets and specific marker genes, including B cells, basophils, erythroblasts, granulocytes, hematopoietic stem cells (HSCs), mesenchymal stem cells (MSCs), macrophages, mast cells, monocytes, and T cells (Fig. 5B). Each cell type was distinguished by specific marker gene expression: (1) Erythroblasts (clusters 8 and 17) expressed *Bpgm*, *Hbb-bs*, and *Hbb-bt*; (2) Monocytes (clusters 0, 1, 2, 7, 14) expressed *Cd14*, *Cd68*, and *Fcgr3*; (3) Macrophages (clusters 3, 6, 12) expressed *Cd68*, *Mpeg1*, and *C1qc*; (4) B cells (cluster 11) expressed *Cd79a*, *Cd79b*, and *Cd19*; (5) Basophils (clusters 4 and 10) expressed *Ccl3*, *Mcpt8*, and *Fcer1a* (Fig. 5C). The distribution of marker genes was visualized in a t-SNE plot to further confirm cell types (Fig. 5D), and the proportions and distributions of different cell types were summarized (Fig. 5E).

Differential gene function enrichment analysis of erythroblasts in various groups

Differential gene expression across the WT, MDS model, and Realgar treatment groups reflects distinct disease and drug interactions, including comparisons of WT vs. NHD13 and Realgar vs. NHD13. The WT vs. NHD13 analysis aids in exploring regulatory pathways underlying MDS, while the Realgar vs. NHD13 comparison reveals

the drug's effect on erythroblast differentiation. Volcano plots illustrate DEGs, with the top 10 genes ($P < 0.05$, $|\text{Log}_2 \text{FC}| > 0.25$) highlighted. In the WT vs. NHD13 comparison, 996 genes are downregulated, including *Cstcd5*, *Cstcd4*, and *Staf1*. Similarly, 711 genes are downregulated in the Realgar vs. NHD13 comparison, with *Cstcd5*, *Cstcd4*, and *Staf1* showing reduced expression (Fig. 6A). Gene Set Enrichment Analysis (GSEA) revealed that genes related to abnormal erythroid precursor numbers and erythroid hypoplasia were upregulated in the NHD13 group but downregulated in the Realgar group. Additionally, antioxidant activity-related genes were upregulated in the Realgar group (Fig. 6D). The overlap of upregulated genes in the WT vs. NHD13 and Realgar vs. NHD13 comparisons was analyzed using a Venn diagram, identifying 17 overlapping genes, including *Lmna*, *Hbb-a1*, *Hbb-y*, and *Snca* (Fig. 6B, Supplementary Table S12). To further elucidate the biological functions of Realgar in regulating erythroblasts, GO and KEGG analyses were performed on the upregulated genes in the Realgar vs. NHD13 comparison. GO analysis revealed enrichment in functions such as oxygen binding, hemoglobin complex formation, and oxygen carrier activity, while KEGG analysis highlighted the IL-17 signaling pathway (Fig. 6C, E).

Single-cell transcriptome analysis of mouse bone marrow cells cultured with As_2S_2 was also conducted. The volcano plot revealed 1401 upregulated genes and 599 downregulated genes between the As_2S_2 and Control groups (Fig. 7A). GO analysis of the upregulated genes indicated enrichment in processes such as erythrocyte differentiation and regulation of MAP kinase activity (Supplementary Fig. S6 A). KEGG pathway analysis identified significant involvement of the IL-17 and MAPK pathways (Fig. 7B).

Overlapped differential gene function enrichment analysis between in vivo and in vitro experiments

To further elucidate the mechanism by which Realgar influences erythropoiesis, single-cell transcriptome sequencing data from both in vivo and in vitro mouse models were integrated. By intersecting the upregulated and downregulated genes across the datasets, common DEGs were identified. GO and Reactome enrichment

(See figure on next page.)

Fig. 7 Enrichment analysis of differentially expressed genes in erythroblasts in vitro and analysis of the intersection of in vivo and in vitro differentially expressed genes. **(A)** Volcano plot displaying DEGs, with red dots representing significantly upregulated genes ($P \leq 0.05$, $|\text{Log}_2 \text{FC}| \geq 0.25$) and blue dots indicating significantly downregulated genes ($P \leq 0.05$, $|\text{Log}_2 \text{FC}| \geq 0.25$). The top 10 DEGs are labeled. **(B)** KEGG enrichment analysis of upregulated DEGs in the As_2S_2 vs. Control comparison. **(C)** Venn diagram showing the overlap of upregulated DEGs in erythroblasts between Realgar vs. NHD13 (in vivo) and As_2S_2 vs. Control (in vitro) comparisons, with 17 overlapping genes identified. **(D)** GO enrichment analysis of the overlapping upregulated genes. **(E)** KEGG enrichment analysis of the overlapping upregulated genes. **(F)** Reactome enrichment analysis of the overlapping upregulated genes

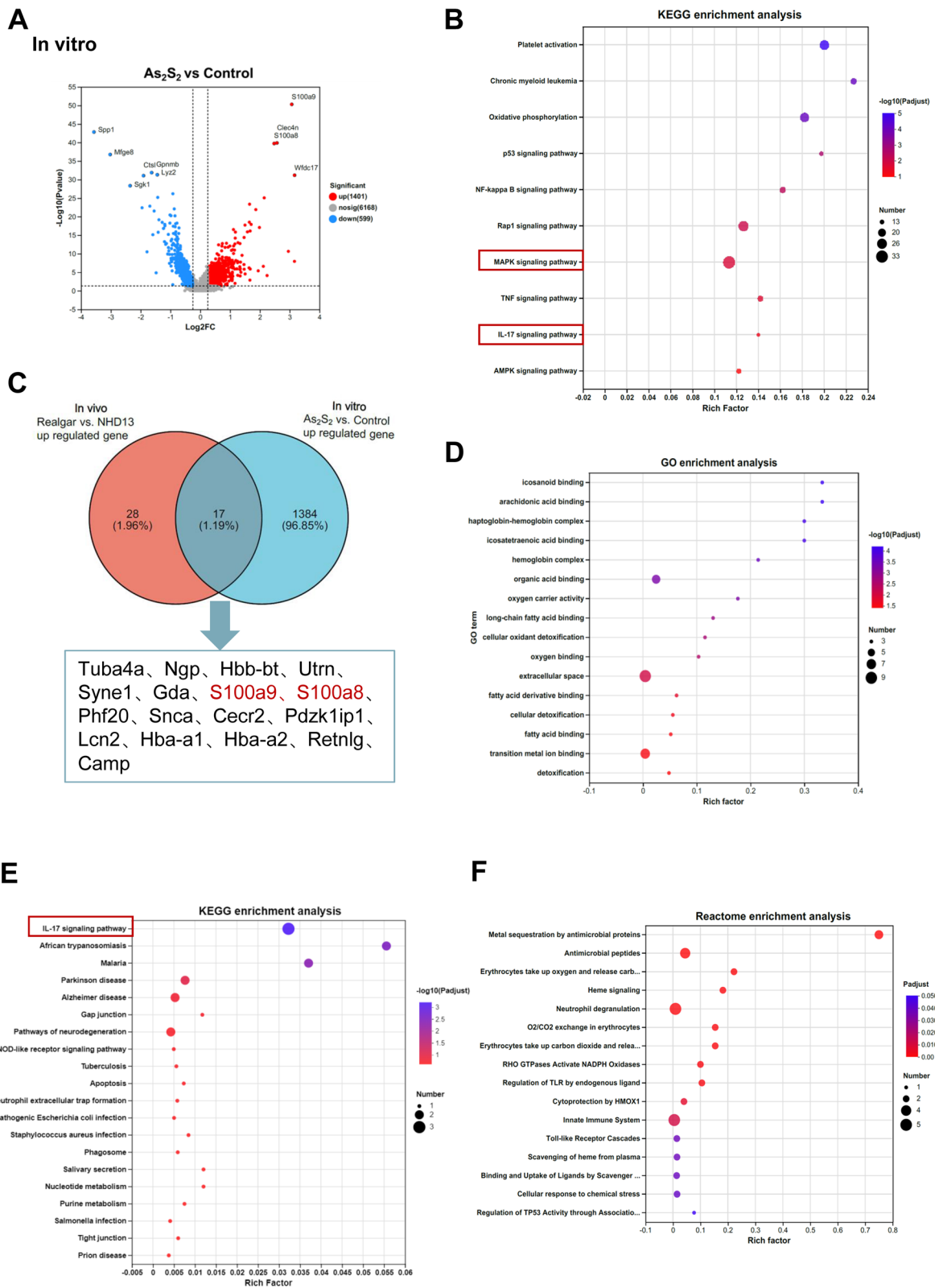


Fig. 7 (See legend on previous page.)

analyses were then performed to refine functional insights and enhance data reliability. The overlap of upregulated genes from both experiments yielded 17 genes commonly upregulated (Fig. 7C, Supplementary Table S13). GO analysis revealed significant enrichment in functions such as oxygen binding, hemoglobin complex formation, and oxygen carrier activity (Fig. 7D), which aligned closely with previous findings, reinforcing the validity of these terms. Reactome pathway analysis identified 58 enriched pathways (FDR < 0.05), with notable pathways including “Erythrocytes take up oxygen and release carbon dioxide,” “Heme signaling,” and “O₂/CO₂ exchange in erythrocytes” (Fig. 7F). Additionally, KEGG enrichment highlighted the IL-17 signaling pathway, consistent with earlier results (Fig. 7E). Conversely, 103 common downregulated genes were identified, and GO analysis showed enrichment in processes such as ribosomal small subunit biogenesis, mRNA 5′-UTR binding, and ubiquitin ligase inhibitor activity (Supplementary Fig. S6B). Further Reactome and KEGG pathway analyses revealed 19 enriched pathways (FDR < 0.05), primarily involving “Major pathway of rRNA processing in the nucleolus and cytosol,” “rRNA processing in the nucleus and cytosol,” and “rRNA processing” (Supplementary Fig. S6 C, D). These results suggest that Realgar may enhance erythrocyte hemoglobin synthesis and oxygen-carrying capacity by upregulating the IL-17 signaling pathway, ultimately boosting red blood cell precursor numbers and promoting erythropoiesis.

Experimental validation of bioinformatics results

To validate the bioinformatics findings, WB analysis was conducted to assess the protein expression of key molecules in the IL-17 signaling pathway regulated by Realgar. Based on the *in vivo* single-cell transcriptome data, Realgar was found to significantly modulate the expression of S100a8 and S100a9, which are involved in the IL-17 signaling pathway (Fig. 8A). Following this, Ter119⁺ cells were enriched from bone marrow samples using magnetic bead isolation, and WB confirmed that S100a8 and S100a9 protein levels were significantly increased in Ter119⁺ cells from the Realgar-treated group (Fig. 8B, C). Additionally, the involvement of the ERK1/2 pathway,

a key component of the MAPK signaling cascade, in Realgar-induced erythroid differentiation was further investigated. Bone marrow cells cultured *in vitro* were treated with varying concentrations of the ERK1/2 pathway inhibitor U0126. WB analysis demonstrated effective inhibition of ERK1/2 pathway activation by U0126 (Fig. 8D, E). Flow cytometry results showed that Realgar-induced erythroid differentiation was significantly reduced upon inhibition of the ERK1/2 pathway (Fig. 8F, G).

Discussion

Realgar, a traditional Chinese mineral medicine, is recognized for its diverse therapeutic properties, including anti-tumor, anti-inflammatory, and anti-parasitic effects, with particular efficacy against hematologic malignancies such as AML, making it a prominent subject of recent research. Previous studies have demonstrated that Realgar can inhibit the proliferation of MDS cells, induce tumor apoptosis, and upregulate the erythroid transcription factor GATA1. However, the precise mechanism underlying its effects remains unclear. This study focuses on elucidating Realgar’s role in ameliorating ineffective hematopoiesis. By employing single-cell transcriptome sequencing and integrating both *in vivo* and *in vitro* datasets, the research aims to explore the impact and potential mechanisms of Realgar on MDS bone marrow erythroid precursor cells.

The study utilized the NUP98-HOXD13 fusion gene mouse model, which replicates the core features of MDS, including peripheral blood cell reduction, bone marrow dysplasia, and progression to acute leukemia. This model mirrors the clinical course of MDS, where all mice ultimately progress to acute leukemia or severe anemia, characterized by reduced white blood cell counts, and succumb within 14 months. This makes it an accurate preclinical model for assessing MDS treatments and investigating underlying biological mechanisms. In this study, 3- to 4-month-old NHD13 model mice were selected, showing a marked reduction in all three blood cell lineages compared to the WT group, confirming the reliability of this model. Following Realgar treatment, significant improvements were observed in the blood

(See figure on next page.)

Fig. 8 Preliminary validation of bioinformatics results. **(A)** Violin plot depicting the expression levels of S100a8 and S100a9 in erythroblasts. Gene expression in the WT group is shown in blue, in the NHD13 group in red, and in the Realgar group in green. Statistical significance is indicated above each gene. **(B)** Western blot analysis of S100a8 and S100a9 protein expression in Ter119⁺ bone marrow cells. **(C)** Quantification of the gray values of the protein bands in panel B. Data are expressed as mean ± SEM (n = 3). **(D)** Western blot analysis of ERK1/2 and pERK1/2 protein expression in mouse bone marrow cells after *in vitro* culture. **(E)** Quantification of the gray values of the protein bands in panel D. Data are expressed as mean ± SEM (n = 3). **(F)** Flow cytometric analysis of CD71 and CD235a expression in erythroblasts. **(G)** Quantification of the percentage of CD71⁺CD235a⁺ populations from the flow cytometry analysis in panel F. Data are expressed as mean ± SEM (n = 3)

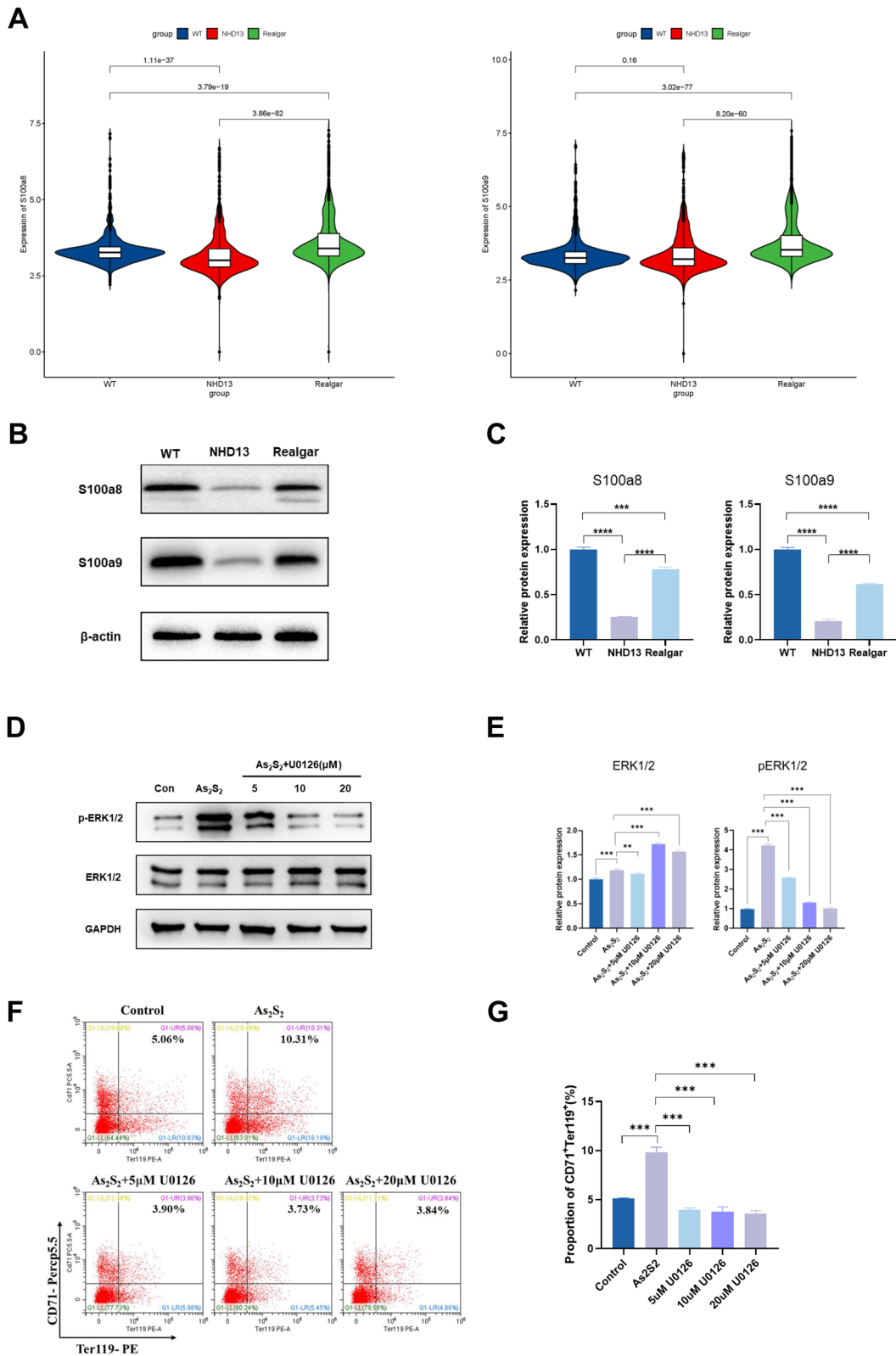


Fig. 8 (See legend on previous page.)

parameters of treated mice, with particularly notable increases in red blood cell counts and hemoglobin levels, in line with previous findings [26]. Given its arsenic content, Realgar's safety was carefully evaluated through tissue histology and weight assessments, confirming the absence of toxicity, thereby affirming its safety profile. The CFU assay is considered the gold standard for evaluating the functionality of hematopoietic stem/progenitor cells in vitro. Research has demonstrated that most patients with MDS exhibit a reduction or complete absence of CFU-E and BFU-E colonies, reflecting impaired differentiation of hematopoietic stem/progenitor cells along the erythroid lineage [31]. In the current study, Realgar treatment increased the number of CFU-E and BFU-E colonies. Flow cytometry analysis further revealed that Realgar predominantly enhanced the number of late-stage erythroid cells at the RII and RIV stages, consistent with previous findings [10]. These results confirm that Realgar can promote late-stage erythroid differentiation and maturation in mouse bone marrow. These results suggest that Realgar can promote late-stage erythroid differentiation and maturation in mouse bone marrow to a significant extent. To determine if Realgar exerts a similar effect in vitro, the study also investigated the impact of its active compound, As₂S₂, on erythroid differentiation in both mouse bone marrow cells and the human K562 cell line. Notably, As₂S₂ continued to promote erythroid differentiation in vitro, indicating that Realgar's therapeutic effects may extend beyond in vivo applications.

To investigate the mechanism of Realgar's action, single-cell transcriptome sequencing was performed to identify overlapping genes associated with diseases and Realgar, alongside DEGs in both in vitro and in vivo settings. This analysis revealed the specific regulatory effects of Realgar on erythropoiesis. The results demonstrated that Realgar positively modulates genes involved in red blood cell hemoglobin synthesis, oxygen affinity, and overall oxygen-carrying capacity. Notably, these genes include *Snca*, *Lcn2*, *Gpx1*, *Hbb-bt*, and *Hbb-y*. *Snca* (alpha-synuclein), primarily expressed in neural tissues and during erythropoiesis, is regulated by the key transcription factor GATA1, a critical player in red blood cell production [32]. *Snca* has been identified as an important regulator of oxidative stress in red blood cells and is essential for hematopoiesis and erythropoiesis in mice. Additionally, serum levels of *Lcn2* are significantly reduced in patients with Mediterranean anemia, suggesting a potential role for *Lcn2* in red blood cell formation [33]. The *Hbb-bt* and *Hbb-y* genes, highly homologous to the human beta-globin gene, are vital for hemoglobin synthesis in mice. *Gpx1*, which encodes glutathione

peroxidase, is a key antioxidant enzyme that protects red blood cells from oxidative stress-induced damage.

Moreover, Realgar may enhance erythroid differentiation through the IL-17 and MAPK signaling pathways. The IL-17 signaling pathway, primarily involved in inflammatory responses, is a key cytokine that links the immune and hematopoietic systems, regulating both homeostasis and stress-induced hematopoiesis [34]. Previous studies have shown that IL-17 mobilizes erythroid progenitor cells from the bone marrow to the spleen, promoting CFU-E differentiation in the spleen to sustain effective erythropoiesis [35]. The S100a8 and S100a9 proteins, central to the IL-17 signaling pathway, have been shown to influence hematopoietic stem and progenitor cell self-renewal and differentiation in NHD13 mice [36]. Our validation experiments confirm that Realgar not only promotes erythroid differentiation but also upregulates the expression of S100a8 and S100a9 proteins. In the *NHD13* MDS model, S100a9 plays a protective role in preventing the progression to AML [36]. Additionally, S100 A9 interacts with TLR4, activating the p38 mitogen-activated protein kinase (MAPK) and the extracellular signal-regulated kinase 1 and 2 (ERK1/2) signaling pathways, which are involved in AML cell differentiation [37]. The MAPK pathway encompasses three primary signaling cascades: MEK/ERK, p38, and JNK, which are integral to a variety of cellular processes [38]. Activation of the MAPK pathway is critical for erythropoiesis, influencing key aspects such as the determination of red blood cell fate, as well as cell proliferation and differentiation [39]. Notably, inhibition of the MEK/ERK pathway with the U0126 inhibitor in human primitive erythrocytes has been shown to prevent nuclear extrusion and impede the formation of cytoplasmic vesicles and transferrin receptor endocytosis, highlighting the critical role of the MEK/ERK pathway in human erythrocyte maturation [40]. Our preliminary experiments indicate that the erythroid differentiation-promoting effect of As₂S₂ is significantly reduced when the ERK1/2 pathway is inhibited. In summary, this study provides a comprehensive single-cell transcriptome profile of Realgar treatment in the MDS mouse model, offering deeper insights into MDS pathophysiology and suggesting a potential mechanism by which Realgar enhances erythropoiesis in this context.

However, this study has several limitations. (1) While this research aims to expand the understanding of Realgar's application in MDS and elucidate its pharmacological mechanisms in erythropoiesis, in-depth investigations of key genes have not been conducted. Future studies will address this gap by exploring the effects of key genes on Realgar's action using techniques such as gene editing and knockout. (2) Our findings suggest the involvement of the IL-17 and MAPK signaling pathways in Realgar

treatment. Further experiments are needed to validate the role of these pathways in mediating the pharmacological effects of Realgar. (3) The sample size of MDS model mice used in our study is limited, which may not fully capture the disease's natural progression. Future research should increase the sample size to improve our understanding of MDS development.

Conclusions

This study demonstrated that Realgar significantly and safely improves blood counts in mice with myelodysplastic syndrome, promoting erythropoiesis. In vitro experiments revealed that As₂S₂, the main active component of Realgar, enhances the expression of erythroid markers and promotes erythroid differentiation. Moreover, this study presented, for the first time, a single-cell transcriptome map of MDS mice and identified DEGs and signaling pathways regulated by Realgar in erythroid precursor cells. Notably, Realgar's promotion of erythroid differentiation may be mediated through the IL-17 and MAPK signaling pathways. These findings offer new insights into the pharmacological effects and mechanisms underlying Realgar's potential as a treatment for MDS. Chemical compounds studied in this article Arsenic(II) sulfide (PubChem CID: 3627253).

Supplementary Information

The online version contains supplementary material available at <https://doi.org/10.1186/s12935-025-03768-0>.

Additional file 1.
Additional file 2.
Additional file 3.

Acknowledgements

We thank Shanghai Majorbio Bio-pharm Technology for providing single-cell sequencing.

Author contributions

HX and JHL conceptualized the study; HX, KXH, and YLW conducted the experiments; SYC and FW contributed to various experimental procedures; JZB and QH analyzed the data and prepared the figures; HX and YG wrote the manuscript; HX, JHL and YCT revised the manuscript and provided final approval for publication. All authors reviewed and approved the final manuscript.

Funding

This work was supported by the National Natural Science Foundation of China (No.82474260), The Leading Talent Project of the Oriental Talent Program (No.2022079), Shanghai Science Technology and Innovation Action Plan (No.21Y31920400), Future planning project of Shanghai Municipal Hospital of Traditional Chinese Medicine(WL-HBMS- 2021009 K).

Data availability

The datasets generated and/or analyzed during the current study are available from the corresponding author on reasonable request.

Declarations

Ethics approval and consent to participate

The animal experiments were approved by the Experimental Animal Ethics Committee of the Municipal Hospital of Traditional Chinese Medicine, Shanghai University of Traditional Chinese Medicine.

Consent for publication

Not applicable.

Competing interests

The authors declare no competing interests.

Received: 16 February 2024 Accepted: 28 March 2025

Published: 8 April 2025

References

- Arber DA, Orazi A, Hasserjian R, et al. The 2016 revision to the World Health Organization classification of myeloid neoplasms and acute leukemia. *Blood*. 2016;127(20):2391–405.
- Fenaux P, Haase D, Santini V, et al. Myelodysplastic syndromes: ESMO Clinical Practice Guidelines for diagnosis, treatment and follow-up(dagger). *Ann Oncol*. 2021;32(2):142–56.
- Ali AM, Huang Y, Pinheiro RF, et al. Severely impaired terminal erythroid differentiation as an independent prognostic marker in myelodysplastic syndromes. *Blood Adv*. 2018;2(12):1393–402.
- Tanno T, Miller JL. Iron loading and overloading due to ineffective erythropoiesis. *Adv Hematol*. 2010;2010:358283.
- Zhu HH, Hu J, Lo-Coco F, et al. The simpler, the better: oral arsenic for acute promyelocytic leukemia. *Blood*. 2019;134(7):597–605.
- Expert Committee on Myelodysplastic Syndromes of Hematology Committee of China Association of Integrative Medicine. Expert consensus of Integrated Medicine for diagnosis and treatment of myelodysplastic syndromes. *Chin J Integr Med*. 2018;38(8):914–20.
- Technical Standards Approval Committee for Hematology of the World Federation of Chinese Medicine Societies. A guideline of clinical practice for Suidulao (myelodysplastic syndrome). A guideline of clinical practice for Suidulao (myelodysplastic syndrome). 2019;41(4):4.
- Hu XM, Tanaka S, Onda K, et al. Arsenic disulfide induced apoptosis and concurrently promoted erythroid differentiation in cytokine-dependent myelodysplastic syndrome-progressed leukemia cell line F-36p with complex karyotype including monosomy 7. *Chin J Integr Med*. 2014;20(5):387–93.
- Hua HY, Gao HQ, Sun AN, et al. Arsenic trioxide and triptolide synergistically induce apoptosis in the SKM1 human myelodysplastic syndrome cell line. *Mol Med Rep*. 2016;14(5):4180–6.
- Fan T, Feng X, Yokota A, et al. Arsenic dispensing powder promotes erythropoiesis in myelodysplastic syndromes via downregulation of HIF1A and upregulation of GATA factors. *Am J Chin Med*. 2021;49(2):461–85.
- Tingting XUE, Yuchen TAO, Jiahui LU. Realgar promoting apoptosis of myelodysplastic syndrome cells through STAT3/GLUT1 signaling pathway. *Shanghai J Tradition Chin Med*. 2023;57(12):88–95.
- Hu XM, Yuan B, Tanaka S, et al. Arsenic disulfide-triggered apoptosis and erythroid differentiation in myelodysplastic syndrome and acute myeloid leukemia cell lines. *Hematology*. 2014;19(6):352–60.
- Ye HQ, Gan L, Yang XL, et al. Membrane-associated cytotoxicity induced by realgar in promyelocytic leukemia HL-60 cells. *J Ethnopharmacol*. 2006;103(3):366–71.
- Xu M, Ren JY, Guo YC, et al. Effects of arsenic disulfide on apoptosis, histone acetylation, toll like receptor 2 activation, and erythropoiesis in bone marrow mononuclear cells of myelodysplastic syndromes patients in vitro. *Leuk Res*. 2017;62:4–11.
- Han X, Wang R, Zhou Y, et al. Mapping the mouse cell atlas by microwell-seq. *Cell*. 2018;173(5):1307.
- Din H. *Experimental pharmacology [M]*. Beijing: Science Press; 2008. p. 73.

17. Le DT, Durham JN, Smith KN, et al. Mismatch repair deficiency predicts response of solid tumors to PD-1 blockade. *Science*. 2017;357(6349):409–13.
18. Satija R, Farrell JA, Gennert D, et al. Spatial reconstruction of single-cell gene expression data. *Nat Biotechnol*. 2015;33(5):495–502.
19. Stuart T, Butler A, Hoffman P, et al. Comprehensive integration of single-cell data. *Cell*. 2019;177(7):1888–1902.e21.
20. Van Der Maaten L, Hinton G. Visualizing data using t-SNE. *J Mach Learn Res*. 2008;9(11).
21. Blondel VD, Guillaume J-L, Lambiotte R, et al. Fast unfolding of communities in large networks. *J Stat Mech Theor Exp*. 2008;2008(10):P10008.
22. Zhang Z, Luo D, Zhong X, et al. SCINA: a semi-supervised subtyping algorithm of single cells and bulk samples. *Genes*. 2019;10(7):531.
23. Lin YW, Slape C, Zhang Z, et al. NUP98-HOXD13 transgenic mice develop a highly penetrant, severe myelodysplastic syndrome that progresses to acute leukemia. *Blood*. 2005;106(1):287–95.
24. Beachy SH, Aplan PD. Mouse models of myelodysplastic syndromes. *Hematol Oncol Clin North Am*. 2010;24(2):361–75.
25. Kogan SC, Ward JM, Anver MR, et al. Bethesda proposals for classification of nonlymphoid hematopoietic neoplasms in mice. *Blood*. 2002;100(1):238–45.
26. Tao YC, Lu JH, Wang DQ, et al. Efficacy and safety of compound arsenic trioxide in mice with myelodysplastic syndrome and its effect on intestinal flora. *China J Trad Chin Med Pharm*. 2022;37(05):2541–7.
27. Lim M, Brown HM, Rose RD, et al. Dysregulation of bisphosphoglycerate mutase during in vitro maturation of oocytes. *J Assist Reprod Genet*. 2021;38(6):1363–72.
28. An X, Schulz VP, Li J, et al. Global transcriptome analyses of human and murine terminal erythroid differentiation. *Blood*. 2014;123(22):3466–77.
29. Liu J, Han X, An X. Novel methods for studying normal and disordered erythropoiesis. *Sci China Life Sci*. 2015;58(12):1270–5.
30. Cantù C, Ierardi R, Alborelli I, et al. Sox6 enhances erythroid differentiation in human erythroid progenitors. *Blood*. 2011;117(13):3669–79.
31. Kang SH, Perales O, Michaud M, et al. BOK promotes erythropoiesis in a mouse model of myelodysplastic syndrome. *Ann Hematol*. 2019;98(9):2089–96.
32. Renella R, Schlehe JS, Selkoe DJ, et al. Genetic deletion of the GATA1-regulated protein α -synuclein reduces oxidative stress and nitric oxide synthase levels in mature erythrocytes. *Am J Hematol*. 2014;89(10):974–7.
33. Weizer-Stern O, Adamsky K, Amariglio N, et al. Downregulation of hepcidin and haemojuvelin expression in the hepatocyte cell-line HepG2 induced by thalassaemic sera. *Br J Haematol*. 2006;135(1):129–38.
34. Mojsilović S, Jauković A, Santibañez JF, et al. Interleukin-17 and its implication in the regulation of differentiation and function of hematopoietic and mesenchymal stem cells. *Mediators Inflamm*. 2015;2015:470458.
35. Monteiro JP, Benjamin A, Costa ES, et al. Normal hematopoiesis is maintained by activated bone marrow CD4⁺ T cells. *Blood*. 2005;105(4):1484–91.
36. Chen BY, Song J, Hu CL, et al. SETD2 deficiency accelerates MDS-associated leukemogenesis via S100a9 in NHD13 mice and predicts poor prognosis in MDS. *Blood*. 2020;135(25):2271–85.
37. Laouedj M, Tardif MR, Gil L, et al. S100A9 induces differentiation of acute myeloid leukemia cells through TLR4. *Blood*. 2017;129(14):1980–90.
38. Garrington TP, Johnson GL. Organization and regulation of mitogen-activated protein kinase signaling pathways. *Curr Opin Cell Biol*. 1999;11(2):211–8.
39. Kumkhaek C, Aerbajinai W, Liu W, et al. MASL1 induces erythroid differentiation in human erythropoietin-dependent CD34⁺ cells through the Raf/MEK/ERK pathway. *Blood*. 2013;121(16):3216–27.
40. An C, Huang Y, Li M, et al. Vesicular formation regulated by ERK/ MAPK pathway mediates human erythroblast enucleation. *Blood Adv*. 2021;5(22):4648–61.

Publisher's Note

Springer Nature remains neutral with regard to jurisdictional claims in published maps and institutional affiliations.